MATHEMATICAL MODEL FOR COMBINED EFFECT OF SEI FORMATION AND GAS EVOLUTION IN LI-ION BATTERIES

Muhammad Rashid* and Amit Gupta**,[1]

Department of Mechanical Engineering, Indian Institute of Technology Delhi, New Delhi 110016, INDIA

*Electrochemical Society Student Member
**Electrochemical Society Member
[1]Corresponding author. Email: agupta@mech.iitd.ac.in

ABSTRACT

In this study, a mathematical model to investigate the combined effect of SEI film formation and gas evolution over the degradation of Li-ion cells is developed. A Li-ion cell is simulated for three discharge/charge rates until 80% of the rated capacity is irreversibly lost in side reactions. The model shows that the thickness of SEI film and volume of gases evolved is between 0.03-0.22 μm and 1.6-10.6%, respectively. It is shown that, in addition to greater diffusion limitations, capacity degradation at higher cycling rates is faster due to reduction in cyclable lithium caused by its accumulation in the negative electrode.

KEYWORDS

Li-ion battery, degradation, gas evolution, SEI formation.

Recent developments in Li-ion batteries (LIBs) have projected them to dominate the automotive sector due to their high gravimetric and volumetric energy density[1]. However, life of LIBs is limited due to fading of capacity of these energy storage systems with repeated cycling. Various side-reactions take place as the ions of lithium travel from one electrode to another through the electrolyte phase, some of which are electrolyte decomposition, passive film formation, gas evolution and active material dissolution[2,3]. These unwanted reactions consume active material and electrolytes, forming an insoluble solid and some liquid and gaseous products[2-5]. The formation of a different gases at each electrode also depends on whether the cell is being charged or discharged. For instance, CO, C_2H_4, CO_2, and H_2 are formed at negative electrode due to electrolyte reduction, whereas electrolyte oxidation produces CO_2 at the positive electrode[3,6]. The formation of gas in a Li-ion battery can lead to (i) swelling and pressure build-up inside the battery, and (b) loss of contact between electrode particles and reduction in the electrolyte volume fraction inside the porous electrode[3] (as is shown in Fig. 1). This reduction in electrolyte volume fraction limits the diffusion of Li-ions through the electrolyte phase, thereby increasing the cell resistance and ohmic losses.

In the past, some experimental and numerical work has been carried out to understand the influence of electrolyte decomposition-based SEI (solid electrolyte interphase) formation over capacity fading of LIBs[4-12]. Methekar et al.[13] simulated the formation of passive film across the anode and concluded that slower charging rates result in slower growth rate of the SEI film. However, it has been suggested that the formation of SEI occurs in tandem with the generation of gas in LIBs as part of the electrolyte decomposition reaction, which for ethylene carbonate (EC) as an electrolyte is given by[2]

$$2EC + 2e^- + 2Li^+ \rightarrow CH_2(OCO_2Li)CH_2(OCO_2Li)\downarrow + C_2H_4\uparrow \quad (1)$$

With this consideration, it was shown that the generation of gases in LIBs can be controlled by adding Li_2CO_3 as an electrolyte additive[6]. Another work demonstrated the evolution of gases in various cathode materials under normal and overcharged conditions[14]. In a recent study, an SEI layer based reduced-order model has been developed[9] to quantify performance faster than differential models for its obvious usage towards operational control[9,10]; however, it does not consider any gas generation inside the battery. Although porosity change caused by deposits on the anode has been studied previously[15,16] , the formation of gas was ignored in these studies as well. A thermo-electrochemical model to quantify the effect of gas evolution was developed to observe the impact of gas volume fraction (and corresponding decrease in electrolyte volume fraction) over a typical cell performance[3]. This quasi-steady model demonstrated the effect of overall gas formation over battery performance, rather than continuous gas generation and its impact on discharge capacity with increasing number of cycles. The influence of spatially varying volume fraction over ohmic drop across the porous electrode has also been studied[17]. However, no work has been directed towards identifying the impact of concurrent gas generation and formation of SEI on the negative electrode over the transport properties of electrodes and cycling performance of LIBs with repeating discharge and charge cycles. Thus, the specific objectives of this work are:

a. Development of an SEI film formation and gas evolution based cyclic degradation model of LIBs, and
b. To quantify the reduction in electrolyte volume fraction due to SEI and gas volume fraction, and its impact over battery discharge capacity and performance as a function of cycle number.

Mathematical model

Details of the ideal-cell isothermal model, which follows the porous-electrode and concentrated-solution theory, is given in earlier papers[18,19] and is not repeated here. In this

section, the mathematical formulation of SEI formation and gas evolution and their coupling with the electrochemical model are presented.

The reduction of the electrolyte at the anode, such as EC and as given in equation (1), is known to produce insoluble alkyl carbonates and ethylene gas. This insoluble alkyl carbonate deposits over anode particles to form a thin SEI film. The formation of a low conductivity film at the anode increases resistance for Li diffusion, whereas gaseous products behave like inert materials and reduce the electrolyte volume fraction[3]. To capture these two interdependent events, the parasitic reaction current density of the electrolyte decomposition reaction can be considered to follow the cathodic Tafel kinetics[11,12]

$$J_{para} = -a_n j^0_{para} \exp\left(\frac{\alpha_{c,n} F}{RT} \eta_{para}\right) \tag{2}$$

where

$$\eta_{para} = \varphi_s - \varphi_e - U_{para} - \frac{J}{a_n} R_{sei} \tag{3}$$

The fraction of volume of solid deposit in the form of SEI film and gases produced by electrolyte decomposition reaction at anode can be written as[4]

$$\frac{\partial \varepsilon_i}{\partial t} = -\frac{J_{para} V_i}{nF} \tag{4}$$

where subscript ‘i’ stands for solid deposit (sd) or gases (g). The actual volume changes in a cell could be predicted by determining the deformation of the cell casing by prescribing the gas pressure as a loading on the structure. To reduce model complexity, the physical model has been simplified by taking the cell volume as fixed; instead the gas formed is assumed to occupy the pore-space in the negative electrode. Thus, the volume occupied by precipitated solid at each particle can be written as

$$V_{sd} = \frac{\varepsilon_{sd} V_p}{\varepsilon_s} \tag{5}$$

The volume of the solid phase (i.e., including SEI) can be written as $V_{sei} = V_p + V_{sd}$. Combining with eqn. (5) and on simplification, the radius of the solid phase will be given by

$$r_{sei} = r_n \left(1 + \frac{\varepsilon_{sd}}{\varepsilon_s} \right)^{1/3} \tag{6}$$

Thus, the thickness of the SEI film ($\delta_{sei} = r_{sei} - r_n$) can be expressed as

$$\delta_{sei} = r_n \left[\left(1 + \frac{\varepsilon_{sd}}{\varepsilon_s} \right)^{1/3} - 1 \right] \tag{7}$$

and the resistance of the film will be

$$R_{sei} = \frac{\delta_{sei}}{\kappa_{sei}} \tag{8}$$

The instantaneous electrolyte volume fraction due to film formation and gas generation is given by

$$\varepsilon_e = \varepsilon_e^0 - \varepsilon_{sd} - \varepsilon_g \tag{9}$$

The volume occupied by the generated gas and SEI film is perceived to depend over various parameters such as electrolyte potential, solid phase potential, applied current and the exchange current density of the parasitic reaction. However, in the literature a lack of clarity prevails regarding the dependence of exchange current density of parasitic reaction on applied current due to dearth of experimental and analytical procedures to quantify the relationship. In other words, the exchange current density has only been reported for a fixed value of charging (typically 1C). However, it is known that parasitic reactions dominate (and parasitic reaction density increases) as the charging rate increases. Due to these reasons, the dependence of the

exchange current density on applied current has been approximated in this study by a non-linear relationship given by

$$j^0_{para} = j^0_{1C}\left(\frac{i_{app}}{i_{1C}}\right)^m \tag{10}$$

where j^0_{1C} is fixed to be 4×10^{-7} A/m^2 [11,12] and m is assumed to be 0.5.

These equations, together with the pseudo-2D electrochemical model[18,19], comprise the governing equations for the degradation model. To solve this set of differential, algebraic and non-linear coupled equations, the finite-element based solver COMSOL Multiphysics was employed with a total of 79 two-noded, one-dimensional elements across the cell domain. A direct solver capable of supporting cluster computing has been used for conducting simulations[20]. The CPU time for simulating 1000 cycles at 1C rate on a single core of an i7 processor with 8GB RAM was approx.100 hours.

Results and Discussion

The pseudo-2D model with SEI formation and gas evolution phenomena has been simulated in this work to study the behavior of $LiMn_2O_4$/MCMB cell. The electrolyte used is 1:2 EC:DMC with 2M $LiPF_6$. Open circuit potentials of electrodes and electrolyte transport property have been taken from Doyle et al[21]. For the lithium ethylene carbonate deposited on the anode, the mass density[5] and electronic conductivity[12] have been taken to be 1690 kg/m^3 and 3.79×10^{-7} S/m, respectively. The molar volume of generated gas has been taken as 4×10^{-4} m^3/mol. Other cell parameters are: for the negative electrode (thickness=100 μm, particle size=12.5 μm, ε_e^0 =0.357), for the positive electrode (thickness=183 μm, particle size=8 μm, ε_e^0 =0.444), separator (thickness=52 μm). U_{para} for the parasitic reaction has been taken to be 0.4V[11,12]. As done in practice, the cell has been cycled at different charge-discharge rates within cut off voltages of 4.2V and 3.0V to minimize the effect of overcharge and deep-discharge of the cell.

Each 'cycle' consisted of a constant current discharge (i.e., i_{app}) to the lower cutoff voltage, followed by same current charge (i.e., $-i_{app}$) to the upper cutoff voltage, and finished with a constant voltage charge until the charging current decayed to 1/20th of the 1C current.

Fig. 2 shows the variation of cell potential with capacity at different cycling rates of 1C, 2C and 4C. As the discharge rate increased, the initial cell potential was considerably lower than the OCP, which is also consistent with an earlier work[22]. Based on simulations, the capacity of a 'fresh' cell was calculated as 15.23, 13.32 and 9.16 Ah/m^2 at 1C, 2C and 4C, respectively. As shown in Fig. 2, when cycling the cell under different rates of 1C, 2C and 4C, 80% of the nominal (1C) capacity was lost in 1000th, 350th, and 98th cycle, respectively. This decrease in the number of cycles indicates that the combined SEI-gas formation model captures the increased rate of degradation at higher rates. The results of simulation conducted without considering gas evolution have been shown in the inset of Fig. 2. The discharge capacity of the cell at 1C rate for 1000th cycle was 3.9 and 3.05 Ah/m^2 for only SEI and SEI with gas evolution model, respectively. However, the thickness of the SEI film was nearly equal due to identical charging conditions in both cases.

The variation in space-averaged SEI film thickness with cycle number for different cycling rates is given in Table 1. Also listed are the change in the average volume fraction of the electrolyte and gas generated for different cycling rates. It can be observed that the volume fraction of electrolyte decreases monotonously as it is consumed in the decomposition reaction. Further, the electrolyte reacts with cyclable Li-ions to form an SEI film (whose thickness increases) which is accompanied by the release of gas. Gas evolution and film formation was rapid (albeit for a shorter duration) when the cell was cycled at higher rates of 2C and 4C; however, the overall magnitude is lesser when compared to the 1C rate owing to the shorter time duration for which charging occurred. The average thickness of the SEI film at the end of

cell life was 0.22, 0.095, and 0.033 μm for 1C, 2C and 4C, respectively. The corresponding volume of gas evolved was recorded to be 10.6, 4.5, and 1.6%, respectively, which is an improvement on the fixed 7% volume of gas assumed irrespective of charging rate in an earlier study[3]. The increased rate of capacity fade at higher currents is due to two reasons: (a) the transport limitation of Li-ion diffusion inside the negative electrode and electrolyte, and (b) the reduction in cyclable lithium concentration across the cell.

To explain the reduction in cyclable lithium between the electrodes, the average lithium concentration in the negative electrode at the end of discharge after a few cycles was analyzed and is listed in Table 1. For all rates, it can be noticed that the concentration of lithium in the negative electrode increased continuously with cycling (and decreased for the positive electrode). This increase in solid lithium in the negative electrode was due to the constant current (CC) discharge process. As mentioned earlier, the complete cycle consisted of CC discharge followed by CC and constant voltage (CV) charge. Charging the cell at CV transfers the maximum possible lithium from the positive to the negative electrode, whereas due to CC discharge that much lithium cannot be extracted from the latter electrode. By this way, lithium is accumulated in the negative and depleted from the positive electrode. From Table 1, it is also clear that this phenomenon of reduction in 'cyclable' lithium is rapid in the case of cycling at higher rates and is the prime reason for the rapid cell degradation during high rate cycling.

To highlight the reduction in cell capacity and potential with cycling, the current profile and cell potential for the 1^{st}, 500^{th}, and 1000^{th} cycle at 1C rate are shown in Fig. 3. As the cycle number increased, the cell discharged in a short duration due to substantial drop in electric potential over the SEI film. During the first cycle, the time duration of charging through CC was longer than CV; however, as the cycle number increased, duration of CC decreased and CV increased due to the resistance offered by the SEI film over the negative electrode and diffusion limitations due to the reduction in volume fraction of the electrolyte. As the cycle

number increased further, the internal resistance caused a large potential change across the film, due to which the Li-ion cell ceased to go through the CC charging process. Rather, and as shown in Fig. 3, CV charging began much earlier and continued for a longer time duration until a cut-off current was reached. Moreover, the effect of the SEI film was also felt during the CC discharge portion of every new cycle as the time duration for discharging the cell kept decreasing due to a higher potential drop across the film. This lowering of the discharge duration resulted in a continuous decline in the cell capacity to a point where it dropped by 80% of the starting capacity.

To conclude, a mathematical model has been developed to investigate the combined effect of the SEI film formation and gas evolution over the capacity degradation of Li-ion cells. A rapid loss in cell capacity at high rates was attributed to the reduction in cyclable lithium in the cell. Simulations demonstrated that high rate operation results in increased rates of film and gas formation and rapid capacity loss.

NOMENCLATURE

a_n	specific interfacial area of the negative electrode (m^{-1})
F	Faraday's constant (96,487 C/mol)
i_{app}	applied current (A/m^2)
J	total current density (A/m^3)
J_{para}	parasitic reaction current density (A/m^3)
j^0_{para}	parasitic reaction exchange current denity
n	number of electrons
r_n	particle radius of anode(m)
r_{sei}	particle radius with SEI film (m)
R	universal gas constant (J/mol K)

R_{sei} film resistance (Ω/m^2)

t time (s)

T temperature (K)

U_{para} equilibrium potential of parasitic reaction (V)

V volume (m^3)

V_p volume of active material in the anode (m^3)

$\alpha_{c,n}$ cathodic transfer coefficient of anode

δ_{sei} SEI film thickness (m)

ε_e^0 initial volume fraction of electrolyte

ε_e volume fraction of electrolyte

ε_g volume fraction of gas

ε_{sd} volume fraction of solid deposit

φ_e electrolyte phase potential (V)

φ_s solid phase potential (V)

η_{para} parasitic reaction overpotential (V)

REFERENCES

1. J.M. Tarascon and M. Armand, *Nature*, **414**, 359 (2001).
2. P. Arora, R.E. White, S. Carolina and M. Doyle, *J. Electrochem Soc.*, **145**, 3647 (1998).
3. J.H. Seo, J. Park, G. Plett and A.M. Sastry, *Electrochem. Solid-State Lett.*, **13**, A135 (2010).
4. Y. Dai, L. Cai and R.E. White, *J. Electrochem. Soc.*, **160**, A182 (2012).
5. X. Lin, J. Park, L. Liu, Y. Lee, A. M. Sastry and W. Lu, *J. Electrochem. Soc.*, **160**, A1701 (2013).
6. J. Shin, C. Han, U. Jung, S. Lee, H. Kim and K. Kim, *J. Power Sources*, **109**, 47 (2002).
7. P. Ramadass, B. Haran, P.M. Gomadam, R. White and B.N. Popov, *J. Electrochem. Soc.*, **151**, A196 (2004).
8. M. Broussely, P. Biensan, F. Bonhomme, P. Blanchard, S. Herreyre, K. Nechev and R.J. Staniewicz, *J. Power Sources*, **146**, 90 (2005).
9. A. V. Randall, R.D. Perkins, X. Zhang and G.L. Plett, *J. Power Sources*, **209**, 282 (2012).
10. G.L. Plett, *Electrochem. Solid-State Lett.*, **2**, 63 (2013).
11. G. Ning, R.E. White and B.N. Popov, *Electrochim. Acta*, **51**, 2012 (2006).
12. G. Ning and B.N. Popov, *J. Electrochem. Soc.*, **151**, A1584 (2004).
13. R.N. Methekar, P.W.C. Northrop, K. Chen, R.D. Braatz and V.R. Subramanian, *J. Electrochem. Soc.*, **158**, A363 (2011).
14. W. Kong, H. Li, X. Huang and L. Chen, *J. Power Sources*, **142**, 285 (2005.
15. G. Sikha, B. N. Popov and R. E. White, *J. Electrochem. Soc.*, **151**, A1104 (2004)
16. M. Safari, M. Morcrette, A. Teyssot and C. Delacourt, *J. Electrochem. Soc.*, **156**, A145 (2009).

17. V. Ramadesigan, R.N. Methekar, F. Latinwo, R.D. Braatz and V.R. Subramanian, *J. Electrochem. Soc.,* **157**, A1328 (2010).
18. M. Doyle, T. F. Fuller and J. Newman, *J. Electrochem. Soc.*, **140**, 1526 (1993).
19. T. F. Fuller, M. Doyle and J. Newman, *J. Electrochem. Soc.*, **141**, 1 (1994).
20. P. R. Amestoy, I. S. Duff and J. Y. L'Excellent, *Comput. Methods Appl. Mech. Eng.*, **184**, 501 (2000).
21. M. Doyle, J. Newman, A. S. Gozdz, C. N. Schmutz and J. M. Tarascon, *J. Electrochem. Soc.*, **143**, 1890 (1996).
22. P.W.C. Northrop, V. Ramadesigan, S. De and V.R. Subramanian, *J. Electrochem. Soc.*, **158**, A1461 (2011).

FIGURE CAPTION

Figure 1 Schematic representation of anode before and after cycling.

Figure 2 Voltage vs. capacity for different cycling rates. The inset shows a comparison of results considering (i) only SEI, and (ii) SEI with gas formation when almost 80% capacity is lost due to degradation.

Figure 3 Current and cell potential for 1C rate for different number of cycles. The abscissa has been translated so that the beginning of discharge for each cycle corresponds to time=0.

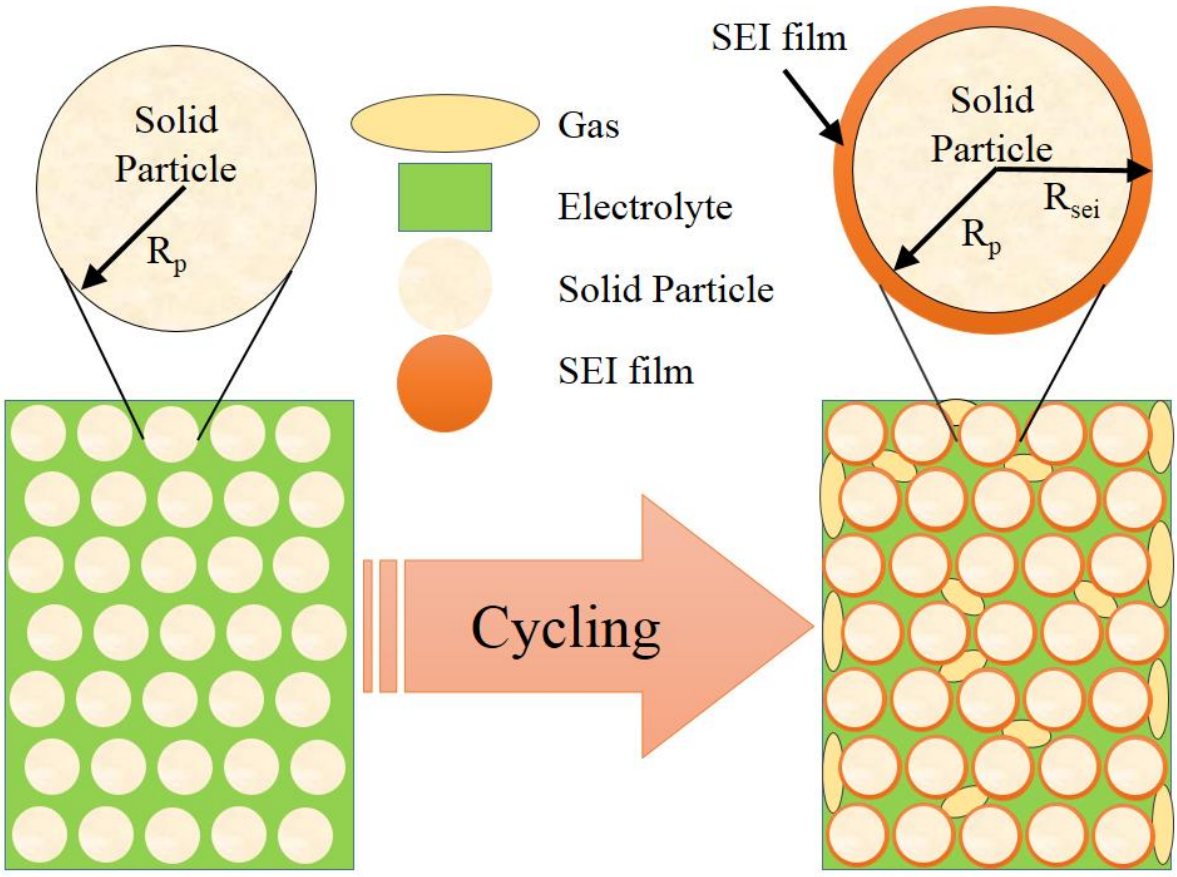
Solid
Particle
R_p
Gas
Electrolyte
Solid Particle
SEI film
SEI film
Solid
Particle
R_{sei}
R_p
Cycling

Figure 1

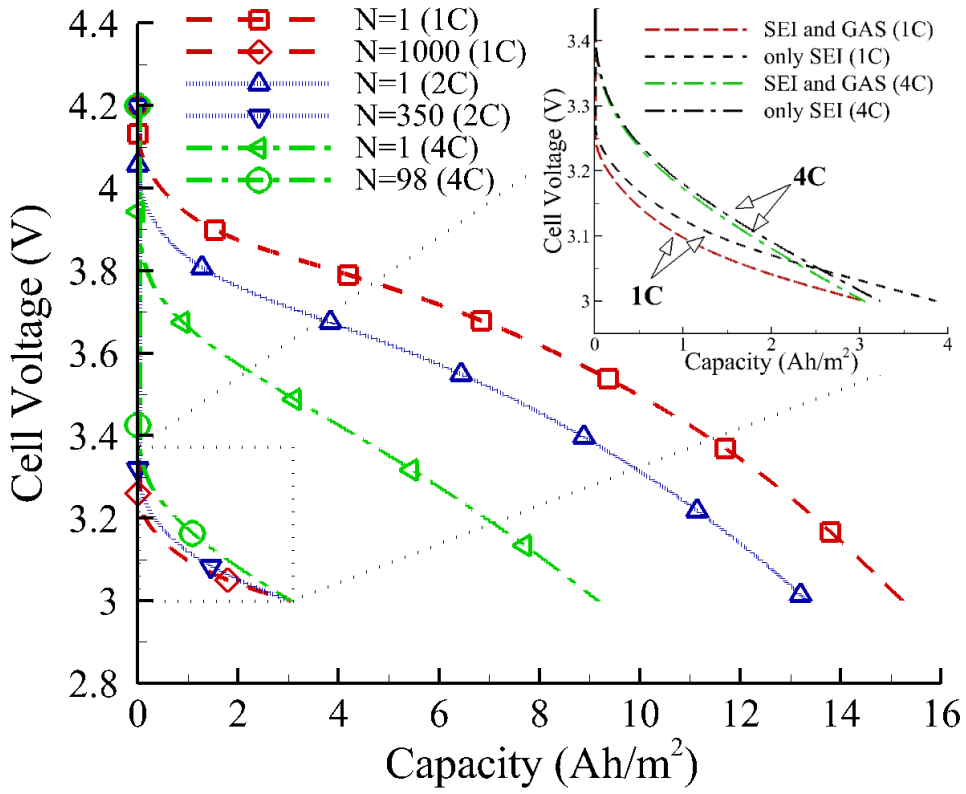
N=1 (1C)
N=1000 (1C)
N=1 (2C)
N=350 (2C)
N=1 (4C)
N=98 (4C)
Cell Voltage (V)
Capacity (Ah/m^2)
SEI and GAS (1C)
only SEI (1C)
SEI and GAS (4C)
only SEI (4C)
4C
1C

Figure 2

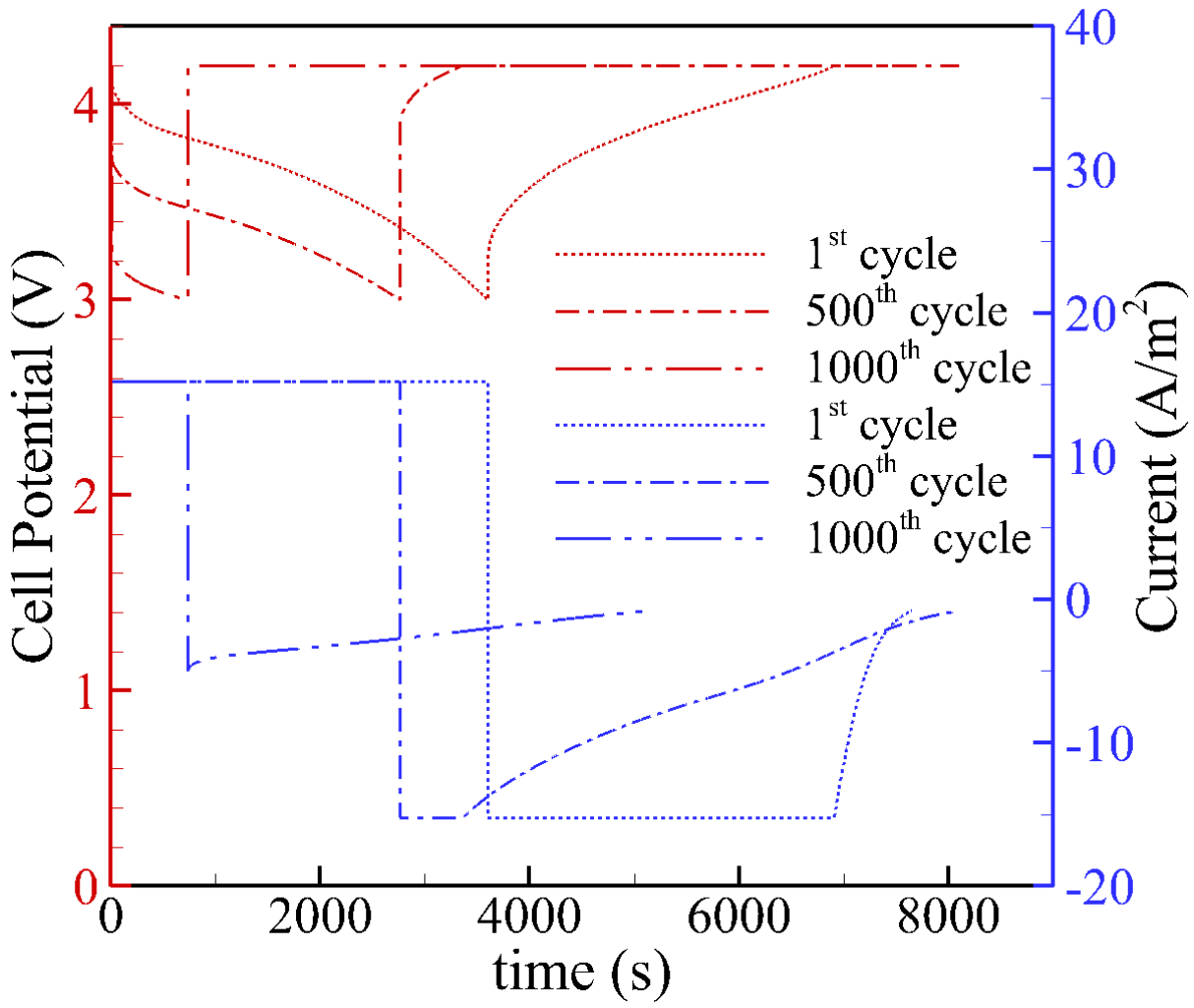
Cell Potential (V)
Current (A/m^2)
time (s)
0
1
2
3
4
0
2000
4000
6000
8000
40
30
20
10
0
-10
-20
1st cycle
500th cycle
1000th cycle
1st cycle
500th cycle
1000th cycle

Figure 3

TABLE CAPTION

Table 1 Various output properties of the cell at the end of discharge as a function of the ongoing cycle number (N) for various rates. For instance, N=500 will mean that cycle 499 is complete and cycle 500 is underway.

Table 1

	N	$\bar{\varepsilon}_g$	$\bar{\varepsilon}_e$	$\bar{\delta}_{sei}$ (nm)	$\bar{c}_{s,neg}$ (M)	$\bar{c}_{s,\mathrm{pos}}$ (M)
Rate	0	0	0.357	0	14.87	3.9
1C	2	8×10^{-5}	0.357	0.2	2.81	14.35
	500	4.57×10^{-2}	0.300	96.1	5.43	12.08
	1000	0.106	0.226	221.0	12.13	6.27
2C	2	1.34×10^{-4}	0.357	0.3	4.33	13.04
	200	2.52×10^{-2}	0.326	53.1	7.76	10.06
	350	4.53×10^{-2}	0.301	95.2	12.27	6.15
4C	2	1.9×10^{-4}	0.357	0.4	7.63	10.17
	60	1.0×10^{-2}	0.345	21.2	10.44	7.74
	98	1.56×10^{-2}	0.338	32.9	12.31	6.12